Applied Catalysis B: Environmental 162 (2015) 381–391

Contents lists available at ScienceDirect

Applied Catalysis B: Environmental

journal homepage: www.elsevier.com/locate/apcatb

A highly efficient photocatalytic H_2 evolution system using colloidal CdS nanorods and nickel nanoparticles in water under visible light irradiation

Shuang Cao [a], Chuan-Jun Wang [a], Xiao-Jun Lv [a,*], Yong Chen [a,*], Wen-Fu Fu [a,b,*]

[a] Key Laboratory of Photochemical Conversion and Optoelectronic Materials and HKU-CAS Joint Laboratory on New Materials, Technical Institute of Physics and Chemistry and University of Chinese Academy of Sciences, Chinese Academy of Sciences, Beijing 100190, PR China
[b] College of Chemistry and Chemical Engineering, Yunnan Normal University, Kunming 650092, PR China

ARTICLE INFO

Article history:
Received 29 April 2014
Received in revised form 3 July 2014
Accepted 6 July 2014
Available online 14 July 2014

Keywords:
Hydrogen production
Visible light
CdS nanorods photosensitizer
Ni nanoparticles catalyst

ABSTRACT

A noble-metal-free photocatalytic system for highly efficient hydrogen production has been developed with colloidal nickel nanoparticles (Ni NPs), CdS nanorods (CdS NRs) and lactic acid (LA) as catalyst, photosensitizer and sacrificial electron donor, respectively, in aqueous solution without any organic solvent. The hydrogen evolution activity of the highly active Ni NPs (6 nm) could amount to 80% of the well-known Pt nanoparticles (5 nm) in equimolar amount at pH 3.0 water solution under visible light ($\lambda \geq 420$ nm) irradiation. A maximum turnover number (TON) of 9710 based on Ni NPs (6 nm) was obtained after 10 h of irradiation at a catalyst concentration of 1.38×10^{-5} M and turnover frequency (TOF) value of 1232 was achieved for the first 6 h of photocatalytic reaction. A series of Ni nanoparticles colloids with different sizes plus Fe, Co nanoparticles were also tested for photocatalytic H_2-evolution. The results showed the obvious effect of Ni NPs size on the hydrogen evolution activity and the smaller (6 nm) Ni nanoparticles exhibited the highest activity compared with other nanoparticles of 11 nm and 20 nm in size. This work demonstrates the size control of non-precious metal nanoparticles could effectively enhance the photocatalytic hydrogen production, which provides an inexpensive means of developing efficient and low-cost photocatalytic systems for harnessing solar energy.

1. Introduction

Hydrogen is the cleanest fuel resource compared to other carbon-based fuels for mitigating the aggravating energy crisis and addressing the worsening environmental issues [1]. Inspired by natural photosynthesis in green plants and bacteria, artificial light-driven water splitting is regarded as one of the most promising ways to solve these exasperating incoming energy and environmental problems [1–5]. Various and innumerable three-component systems containing photosensitizer, sacrificial electron donor and catalyst have been developed over the past two decades for photocatalytic hydrogen evolutions [6–9]. Nanosized semiconductor materials, such as TiO_2, ZnO, ZnS, SnO_2 and others [10–17], having high specific surface areas and providing more active sites which are very important in photocatalytic reactions, have been extensively investigated as both light absorbers and photocatalysts. In comparison with semiconductor photocatalysts, quantum confined semiconductor nanocrystals acting as photosensitizers for photocatalytic hydrogen evolution in aqueous solution have attracted particular attentions due to their excellent light-harvesting and charge-separation activities [18–23]. The featured characteristics of its multiple excitons and electron/hole accumulation sites make quantum confined nanocrystals semiconductor superb candidates as photosensitizers for light-driven hydrogen evolution when coupled with electron donors and efficient catalysts [24].

In addition, compared to light-absorbing molecular chromophores, quantum dots (QDs) usually display some favorable advantages for hydrogen evolution applications such as their controlled size-dependent light absorptions, readily modifiable surfaces, long exciton lifetimes and large extinction coefficients, ability to simultaneously and continuously absorb multiple photons to generate multiple excitons, and their enhanced photostabilities

* Corresponding authors at: Key Laboratory of Photochemical Conversion and Optoelectronic Materials and HKU-CAS Joint Laboratory on New Materials, Technical Institute of Physics and Chemistry and University of Chinese Academy of Sciences, Chinese Academy of Sciences, Beijing 100190, PR China. Tel.: +86 1082543520; fax: +86 1082543520.
E-mail addresses: xjlv@mail.ipc.ac.cn (X.-J. Lv), chenyong@mail.ipc.ac.cn (Y. Chen), fuwf@mail.ipc.ac.cn (W.-F. Fu).

http://dx.doi.org/10.1016/j.apcatb.2014.07.014
0926-3373/

[25–29]. As a result of those superiority qualities, hydrogen evolution systems with QDs sensitizers have attracted widespread interest and displayed enhanced efficiencies and stabilities. Esienberg et al. reported photocatalytic hydrogen-generating system containing CdSe nanocrystal QDs, nickel (II) nitrate and ascorbic acid, and a supreme TONs of 600,000 were achieved with respect to catalyst, which showed the best hydrogen evolution efficiency up to now [18]. In addition, there has been report that the precursor of [FeFe]–H_2ase mimics, $Fe_2S_2(CO)_6$ can interact with CdSe QDs intimately to afford water-soluble CdSe/$Fe_2S_2(CO)_6$ assembly. The stability and activity are the highest known to date for photocatalytic H_2 evolution from [FeFe]–H_2ase mimics system [22,30]. Therefore, these studies provide convincing evidence that semiconductor nanocrystals are favorable photosensitizers for photocatalytic hydrogen evolution from aqueous solution. However, most available water splitting catalysts are still some expensive noble metals (such as Pt, Ru, Ir and Rh) or their complexes, but for real widespread applications, catalysts made from earth abundant and less expensive materials are urgently required [31]. Although Ni, Fe and Co complexes have been used as catalysts in homogeneous systems, their catalytic efficiency is by far lower than that of Pt in most cases [32–34]. Besides, these metal complexes are inherently afflicted by the problem of instability and photodecomposition within a few hours of light irradiation in a mostly organic/water solution [31,35]. Recently, inorganic earth abundant nanoparticles (Ni, Fe, Co) have attracted increasing attention as photocatalysts due to their high catalytic activities and stabilities [21,36–40]. Our previous work demonstrated that Ni nanoparticles in situ generated in a photocatalytic system was an efficient catalyst for H_2-production with organic photosensitizers [41]. Aggregation of nanoparticles resulting in decreased H_2 production activity was observed over prolonged irradiation time, which was improved by incorporating reduced graphene oxide (RGO) to form a dispersed Ni/RGO composite which enhanced the photocatalytic activity to some degree. Fukuzumi et al. reported a photocatalytic hydrogen evolution system with Ni nanoparticles capped with poly(vinylpyrrolidone) as a non-precious metal catalyst, 2-phenyl-4-(1-naphthyl) quinolinium ion (QuPh+–NA) as a photosensitizer, dihydronicotinamide adenine dinucleotide (NADH) as a sacrificial electron donor. The well-dispersed Ni NPs catalyst in their system showed hydrogen evolution rate up to 40% of that catalyzed by Pt nanoparticles when using the same catalyst weight in a mixed MeCN and water solution under UV–vis light irradiation ($\lambda > 340$ nm) [42]. However, quick decomposition of the molecular chromophores under light irradiation greatly reduced the photostability of the system, resulted in the decreased photocatalytic hydrogen production activity. Therefore, it is very imperative to develop a highly efficient system which operates under visible light irradiation and in pure water, which combines the favorable advantages of semiconductor nanocrystals as photosensitizers and well-controlled inorganic earth abundant nanoparticles as catalysts.

Herein, we report a highly efficient and organic-solvent-free photocatalytic hydrogen evolution system for visible light driven ($\lambda \geq 420$ nm) hydrogen production. The system is assembled by using water-soluble colloidal ultrathin CdS nanorods (CdS NRs) as a photosensitizer, size-controlled and well dispersed colloidal nickel nanoparticles (Ni NPs) as a non-precious metal catalyst and lactic acid (LA) as a sacrificial electron donor in water. CdS NRs has been previously reported as one of the potentially promising candidates for visible-light driven photocatalytic water splitting [43–48]. Meanwhile, by exerting size-control over the prepared Ni NPs, aggregation was effectively suppressed and well-dispersed Ni NPs having high specific surface areas was obtained, which would result in enhanced catalytic activity due to the abundantly exposed catalyst active sites. Moreover, these metal colloids can overcome the insolubility problem of common metal nanoparticles to form a "homogeneous" system with CdS NRs. The prepared CdS nanorods and nanoparticles (Ni, Pt, Fe, Co) of various sizes were well-characterized by a series of HRTEM (High resolution transmission electron microscopy), XRD (X-ray diffraction), spectroscopic and DLS (Dynamic light scattering) experiments. A detailed comparison of the photocatalytic hydrogen evolution activity catalyzed by different colloidal metal nanoparticles (Ni, Pt, Co, Fe) and Ni NPs of different sizes (6 nm, 11 nm, 20 nm) were carried out. A Ni NPs size-dependant hydrogen evolution activity relationship was obtained and hydrogen evolution mechanism of electron transfer from CdS NRs to metal nanoparticles was well understood based on a series of similar fluorescence quenching and photocurrent results. The highest photocatalytic activity achieved with the highly active Ni NPs (6 nm) can reach up to 80% of that with Pt NPs in equimolar amount under visible light irradiation at pH 3.0 aqueous solution. The maximum TON of 9710 after 10 h of irradiation and TOF of 1232 h^{-1} for the first 6 h could be achieved, which shows the high efficiency and fast rate of photocatalytic hydrogen evolution in the present Ni NPs catalyzed system. This work manifests a highly efficient photocatalytic hydrogen evolution system combining CdS NRs and earth-abundant nanoparticles and is expected to provide some inspirations on exploring inexpensive means of harnessing solar energy for photocatalytic purposes.

2. Experimental

2.1. Experimental materials

All materials were of analytical grade and used as received without further purification. $Cd(NO_3)_2{\cdot}4H_2O$, thioacetamide, bis(2,4-pentanedionato) nickel(II) [$Ni(acac)_2$], poly(vinylpyrrolidone) (PVP, $M_w = 40{,}000$) were obtained from Sinopharm Chemical Reagent Co. Ltd. (Shanghai, China). Cobalt carbonyl [$Co_2(CO)_8$], iron pentacarbonyl [$Fe(CO)_5$], L-(+)-lactic acid, oleylamine (70%), polyethyleneimine (PEI, $M_w = 70{,}000$, 50 wt% aq. solution), 1-octadecene (ODE, 90%), tri-n-octylphosphine oxide (TOPO) and tri-n-octylphosphine (TOP) were obtained from Alfa Aesar.

2.2. Preparation of water-soluble colloidal CdS nanorods [49]

The water-soluble ultrathin CdS NRs were directly synthesized by a simple hot-injection method using $Cd(NO_3)_2{\cdot}4H_2O$ and thioacetamide as the precursors with the assistance of PEI. Typically, 0.75 g thioacetamide was dissolved in 10 mL ethylene glycol as sulfur precursor solution (1 M). 0.031 g $Cd(NO_3)_2{\cdot}4H_2O$ (0.1 mmol), 0.20 g PEI and 10 mL ethylene glycol was heated to 120 °C under stirring in a 100 mL 3-neck flask. Then 100 μL thioacetamide ethylene glycol stock solution was quickly injected into the hot solution, and the temperature was stabilized at 120 °C for 30 min. When the reaction was cooled to room temperature, the obtained solution was put through dialysis for 24 h to remove the ethylene glycol and excess polymer without further purification (Fig. S1).

2.3. Preparation of 6 nm Ni nanoparticles [50]

$Ni(acac)_2$ (520 mg, 2 mmol) was dissolved in oleylamine (2 mL) in a 3-neck round-bottom flask and heated under an Ar atmosphere at 100 °C to form a metal-complex solution. Then 5 mL TOP was added to the hot solution and heated to 215 °C. The color of the solution was changed from green to black and at this point, the temperature was cooled to 200 °C and kept at this temperature for 30 min. When the solution was cooled to room temperature, ethanol was added to form flocculation and centrifuged to separate

the black precipitates. The obtained black solid was washed by n-hexane/ethanol (1:1) three times.

2.4. Preparation of 11 nm Ni nanoparticles [50]

$Ni(acac)_2$ (257 mg, 1 mmol) and TOP (1.3 mL) were dissolved in oleylamine (7 mL) in a 3-neck round-bottom flask at room temperature. The solution was degassed under an Ar atmosphere at 130 °C for 20 min then heated to 250 °C and kept at this temperature for 30 min. After the solution cooled to room temperature, ethanol was added to form flocculation and centrifuged to separate the black precipitates. The obtained black solid was washed by n-hexane/ethanol (1:1) three times.

2.5. Preparation of 20 nm Ni nanoparticles [50]

$Ni(acac)_2$ (257 mg, 1 mmol) and TOP (0.5 mL) were dissolved in oleylamine (10 mL) in a 3-neck round-bottom flask at room temperature. The solution was degassed under an Ar atmosphere at 130 °C for 20 min then heated to 270 °C and kept at this temperature for 40 min. After the solution cooled to room temperature, ethanol was added to form flocculation and centrifuged to separate the black precipitates. The obtained black solid was washed by n-hexane/ethanol (1:1) three times.

2.6. Preparation of Fe nanoparticles [51]

The mixture of ODE and oleylamine (0.15 mL) was purged with argon at 120 °C. After 20 min, the temperature was raised to 265 °C. Then $Fe(CO)_5$ (0.35 mL) was added and heated for 30 min. After the reaction cooled to room temperature, ethanol (20 mL) was added to form a black precipitates, which can be separated by centrifugation. The obtained black solid was washed by n-hexane/ethanol (1:1) three times.

2.7. Preparation of Co nanoparticles [52]

TOPO (50 mg) was dissolved in a mixture of 1,2-dichlorobenzene (10 mL) and oleic acid (0.10 mL). Then the temperature was heated to 180 °C. $Co_2(CO)_8$ (270 mg) was dissolved in 10 mL 1,2-dichlorobenzene and injected to the mixture and kept 30 min at 180 °C. After the reaction cooled to room temperature, ethanol (20 mL) was added to form a black precipitates, which can be separated by centrifugation. The obtained black solid was washed by n-hexane/ethanol (1:1) three times.

2.8. Preparation of Pt nanoparticles [53]

500 mg PVP and 200 mg L-ascorbic acid (L-AA) were dissolved in 30 mL water and heated to 90 °C. Then 260 mg H_2PtCl_6•$6H_2O$ was added to the solution and kept at this temperature for 3 h. After the solution was cooled to room temperature, acetone was added to cause flocculation and centrifuged to separate the black precipitates. The obtained black solid was washed by acetone/ethanol (1:1) three times.

2.9. Preparation of NiO nanoparticles [54]

0.50 g PVP and 0.25 g $Ni(OAc)_2$•$4H_2O$ were dissolved in 20 mL H_2O and dried up the water at 60 °C in oven. Then the temperature was increased to 100 °C for 1 h. Finally, the mixture was calcined in muffle furnace for 2 h at 450 °C. The product was the NiO nanoparticles.

2.10. Capping agent exchange with PVP [42]

Metal nanoparticles (50 mg) were dissolved in 6 mL n-hexane. A trichloromethane solution containing 500 mg PVP was added to the n-hexane solution and then heated to 65 °C for 12 h under an Ar atmosphere. After the mixture was cooled to room temperature, acetone was added to cause flocculation and centrifuged to separate the black precipitates. The obtained black solid was washed by acetone/ethanol (1:1) three times. The final colloidal metal nanoparticles can be dissolved in water easily to form a transparent and stable solution (Fig. S1).

2.11. Photocatalytic H_2 production activity measurements

The photocatalytic hydrogen-production experiments were performed in a 60 mL quartz tube sealed with a silicone rubber septum. In a typical photocatalytic experiment, the tube containing an aqueous solution of CdS NRs (9.2×10^{-5} M), Ni NPs (5.5×10^{-5} M) and LA (1 mL; 10%, v/v) was adjusted to pH 3.0 with 1 M NaOH and adjusted the total volume of the mixed solution to 10 mL with distilled water. Then the system was deoxygenated with argon for 30 min. LED light source (30×3 W, $\lambda \geq 420$ nm) were used as the irradiation light sources. The LEDs were positioned 2 cm away from the sample which was kept under continuous stirring at room temperature. Hydrogen was measured by a gas chromatograph (GC-14C, Shimadzu, with argon as a carrier gas), which was equipped with a 5 Å molecular sieve column (3 m × 2 mm) and a thermal-conductivity detector. The TON value can be calculated by the formula: $TON = 2n(H_2)/n(cat)$; The TOF value is calculated following the formula: $TOF = 2n(H_2)/[n(cat) \times t]$, n: mole; t: reaction time.

2.12. Photoelectrochemical measurements

Photocurrent measurements were performed on a CHI 660C electrochemical work station (Chenhua Instrument, Shanghai, China) in a conventional three-electrode system. The resultant electrode served as the working electrode, with a platinum wire as the counter electrode and a Ag/AgCl (saturated KCl) electrode as the reference electrode. LED light source (30×3 W, $\lambda \geq 420$ nm) was used as the irradiation light sources. A 0.5 M Na_2SO_4 aqueous solution was used as the electrolyte. The working electrodes were prepared as follows: 20 mg of the prepared anhydrous photocatalyst was ground with 30 μL of a Nafion (5%) aqueous solution and 100 μL of ethanol to make a slurry. The slurry was then spread on a 3.0 cm × 1.0 cm ITO glass substrate with an active area of about 1.0 cm^2. The film was dried at 100 °C for 30 min in a flowing N_2 atmosphere. The photoresponses of the samples as light on and off were measured at 0.0 V.

2.13. Materials characterization

The concentrations of CdS NRs, Ni NPs, Co NPs, Fe NPs and Pt NPs were determined by inductively coupled plasma atom emission spectrometry (ICP-AES, Varian 710-ES, USA). The size, lattice fringes measurements were analyzed on TEM (JEM 2100F) with an accelerating voltage of 200 kV. DLS measurements were performed with a DybaproNanoStar instrument (Wyatt Technology). UV–vis absorption spectra and fluorescence spectral measurements were carried out with a U-3010 (Hitachi) and F-4600 (Hitachi), respectively. XRD pattern was recorded on a Bruker AXS D8 X-ray diffractometer with Cu K_α ($\lambda = 1.54056$ Å).

3. Results and discussion

Fig. 1a shows the typical TEM image of the PEI capped CdS NRs synthesized at 120 °C [49], which is 2.5–5 nm (ultrathin) in

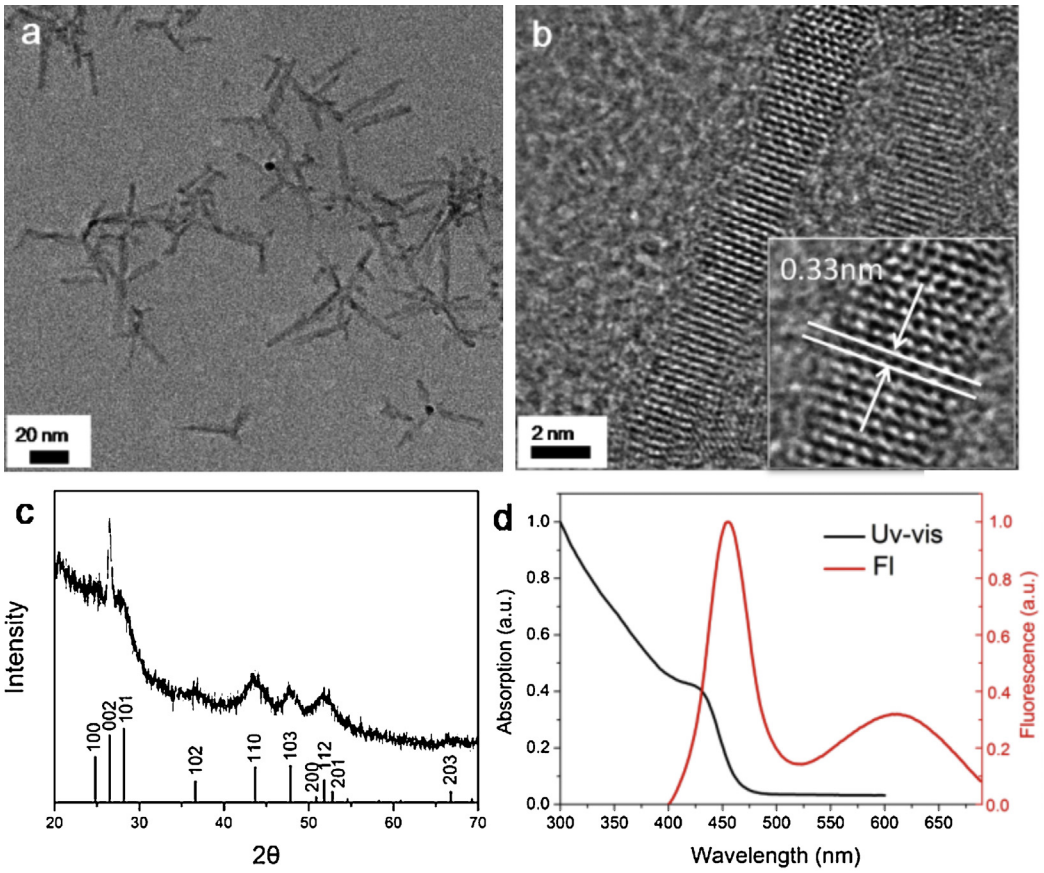

Fig. 1. (a) TEM, (b) HRTEM images, (c) XRD pattern, (d) UV–vis absorption (black line) and fluorescence emission (red line) spectra of the CdS nanorods. (For interpretation of the references to color in text, the reader is referred to the web version of this article.)

diameter and 20–30 nm in length. The lattice fringe with an interplanar spacing of ca. 0.33 nm is ascribed to the (0 0 2) plane of wurtzite CdS (Fig. 1b), indicating that the nanorods grow along the [0 0 1] direction. XRD patterns in Fig. 1c also demonstrate that the as-obtained nanorods are in agreement with the wurtzite phase CdS (JCPDS Card No. 41-1049). It is notable that the (0 0 2) diffraction peak is rather strong and sharp than the others in the XRD pattern, which implies that the CdS nanocrystals preferably grow along the [0 0 2] direction and display rod-like shape [49]. Fig. 1d shows that the UV–vis absorption spectrum of the as obtained CdS NRs has a shoulder peak at ~430 nm. The fluorescence spectrum displays a narrow peak at 450 nm which is attributed to the direct electron–hole recombination. The weak and broad emission at ~600 nm corresponds to the trap-related electron–hole recombination and the surface state emission of the material [49]. The EDS (Energy Dispersive Spectrometer) pattern (Fig. S2) shows the signals of Cd and S, which also confirm the composition of CdS. The signals of Cu and C come from the carbon-coated copper grid substrate.

The different sizes of Ni NPs capped with PVP were easily dissolved in aqueous solution and characterized by TEM, DLS and XRD. The TEM images and DLS measurements revealed that all three kinds of as-synthesized Ni NPs are well-dispersed and size-homogeneous which have a diameter of ca. 6 nm (Fig. 2a–c), 11 nm (Fig. 2d–f) and 20 nm (Fig. 2g–i), respectively. From HRTEM (Fig. 2b, e and h), we can clearly identify the lattice fringes of Ni (0). The d spacing of 0.203 nm can be assigned to the (1 1 1) planes of a face-centered cubic (fcc) Ni crystal. The XRD patterns of the Ni NPs mainly show two broad peaks (Fig. S3). The peaks located at 15–30° and 40–50° belong to the pattern of PVP [54] and Ni NPs [42], respectively.

Smaller nanoparticles can provide a higher specific surface area which offers more catalytic-active sites for photocatalytic H_2-production. And the small particle size and high dispersibility that will secure more efficient charge transfer between Ni nanoparticles and the reactant [55]. Therefore, the different sizes of Ni NPs would have a significant effect on the efficiency of photocatalytic H_2-evolution. In Fig. 3, the photocatalytic H_2-production experiments using different sizes of Ni NPs catalysts were performed and the results demonstrated that Ni NPs with the smallest size (6 nm) exhibited the highest catalytic activity compared to other Ni NPs (11 nm and 20 nm) under the same concentrations of Ni NPs (5.50×10^{-5} M), CdS NRs (1.84×10^{-4} M), LA (1 mL; 10%, v/v) after 10 h of visible light ($\lambda \geq 420$ nm) irradiation in 10 mL pH 3.0 aqueous solution.

Colloidal Pt nanoparticles were also synthesized by reduction of H_2PtCl_6 with L-AA as reducing agent in the presence of PVP for comparison of catalytic activities with Ni NPs. TEM images (Fig. 4a and b) show the size of Pt nanoparticles capped with PVP was ca. 5 nm. The HRTEM image (Fig. 4b) shows a lattice spacing of 0.226 nm, which belongs to the (1 1 1) plane of cubic Pt nanocrystals. DLS measurement (Fig. 4c) clearly shows the obtained Pt NPs with a size of ca. 5 nm. The XRD pattern (Fig. 4d) displays three diffraction peaks which match well with the (1 1 1), (2 0 0) and (2 2 0) reflections of the standard cubic Pt (JCPDS 4-802) [56].

In Fig. 5, we compared the catalytic activity of the synthesized Pt and Ni NPs. The hydrogen evolution amount with the most active Ni NPs (6 nm) has been demonstrated to reach up to 80% that of the well-known Pt NPs (5 nm) using the same catalyst molar amount after 20 h irradiation under the visible light ($\lambda \geq 420$ nm). As shown in Fig. 5, 40.3 mL H_2 and 48.2 mL H_2 is

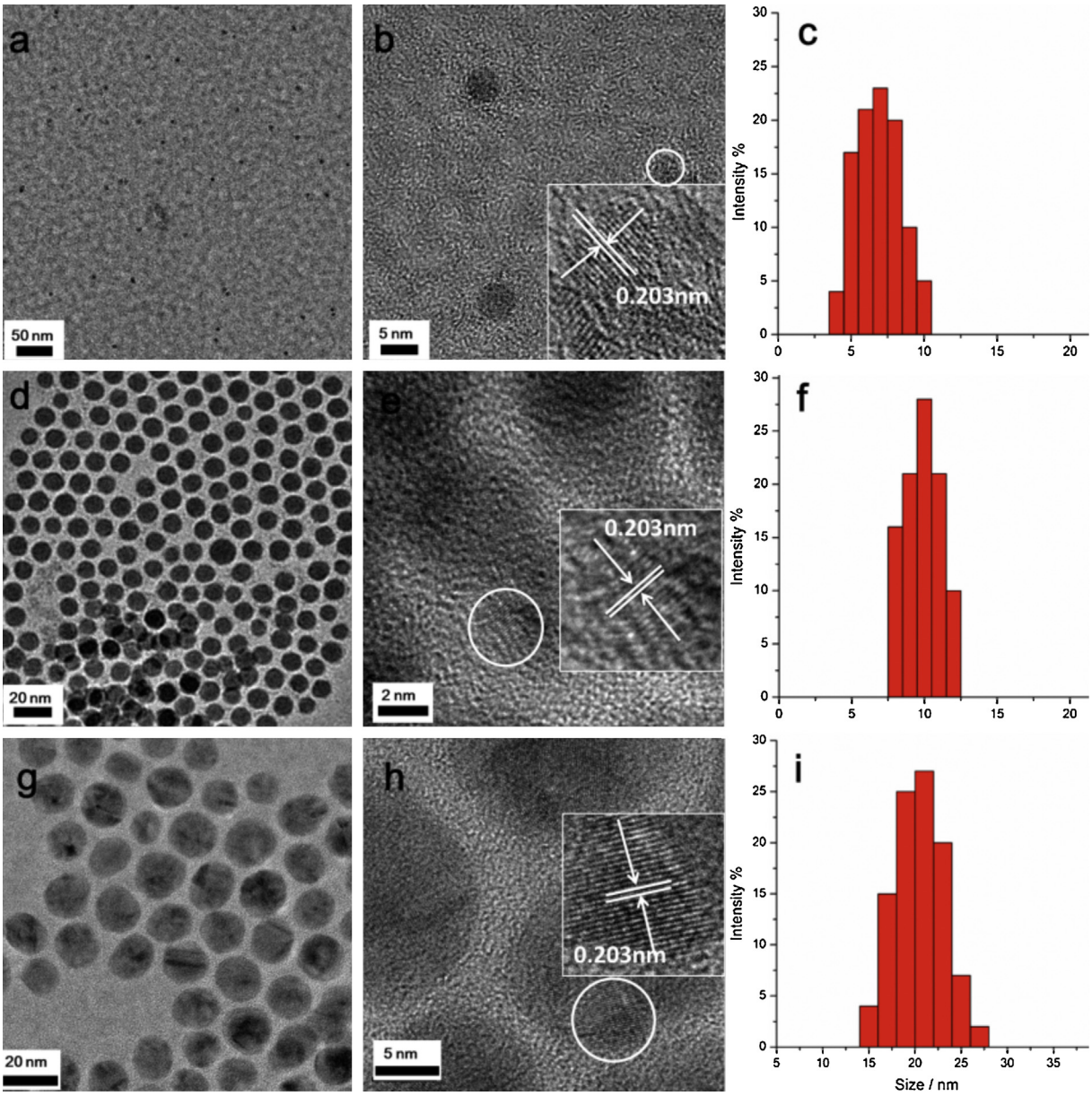

Fig. 2. TEM and HRTEM images of Ni NPs with size of (a and b) 6 nm, (d and e) 11 nm, (g and h) 20 nm; particle size distribution determined by DLS measurements of Ni NPs of (c) 6 nm, (f) 11 nm, (i) 20 nm.

obtained using the same concentration of Ni NPs (6 nm) and Pt NPs (5 nm) catalysts, respectively, containing CdS NRs (1.84×10^{-4} M) photosensitizer, in 10 mL LA water solution (pH = 3.0, adjusted by 1 M NaOH). Considering that Pt is a noble and expensive metal element, the excellent hydrogen evolution efficiency exhibited by the low-cost Ni in the present system is of great economic value and would attract further exploration in developing photocatalysis systems, where earth-abundant metal elements though size-control could match or even rival the activity of Pt NP catalysts of smaller size.

As revealed in our previous work, Ni nanoparticles in situ generated were easily apt to aggregate with the prolonging of irradiation time, which resulted in the decreased photocatalytic activity. Therefore, the approach to synthesis of size-controlled and well-dispersed colloidal water-soluble Ni NPs capped with PVP in this work would offer more active sites on the catalyst due to their relatively large surface areas. Additionally, visible light responsive semiconductor nanocrystal with their favorable characteristics as photosensitizers was also taken advantage in the present work, which in coupling with similar Ni NPs catalyst led to the excellent photocatalytic activity.

A series of control experiments show that several factors could affect the efficiency of H_2 production. It was worth noting that the visible light-driven H_2 production was very dependent on the pH value of the solution, the concentrations of both the CdS NRs and Ni NPs as well. Fig. 6a shows that a maximal rate for H_2 evolution was achieved at pH 3.0, while less amounts of H_2 was obtained at either lower or higher pH values, similar to that in other systems [21,57,58]. The hydrolyzation equilibrium of LA is very sensitive to pH values (p*K*a = 3.86 for LA) [21]. At higher pH values, lactic acid cannot perform as a good electron donor due to the neutralization of the acid and H_2 generation becomes more thermodynamically unfavorable [34]. At lower pH values, Ni NPs can react with lactic acid and become Ni^{2+} more easily. Considering the various affecting factors, an optimized H_2 evolution system was conducted at pH 3.0 based on experimental results.

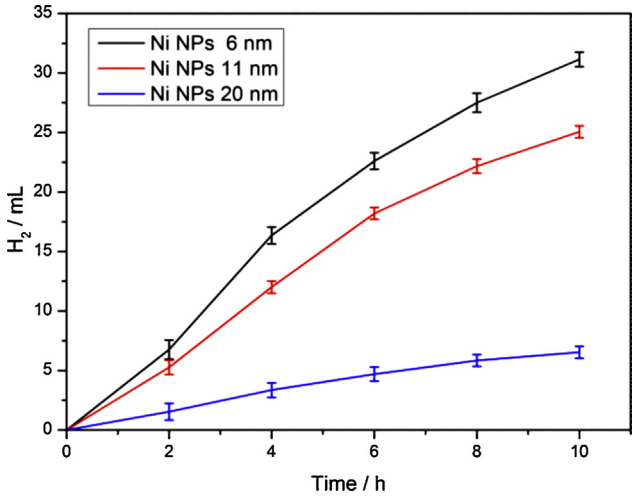

Fig. 3. Photocatalytic hydrogen evolution with different sizes of Ni NPs (6 nm, 11 nm, 20 nm) catalysts under visible light ($\lambda \geq 420$ nm, LED: 30×3 W) irradiation in 10 mL H_2O solution at pH 3.0 containing CdS NRs (1.84×10^{-4} M), lactic acid (1 mL, 10% v/v).

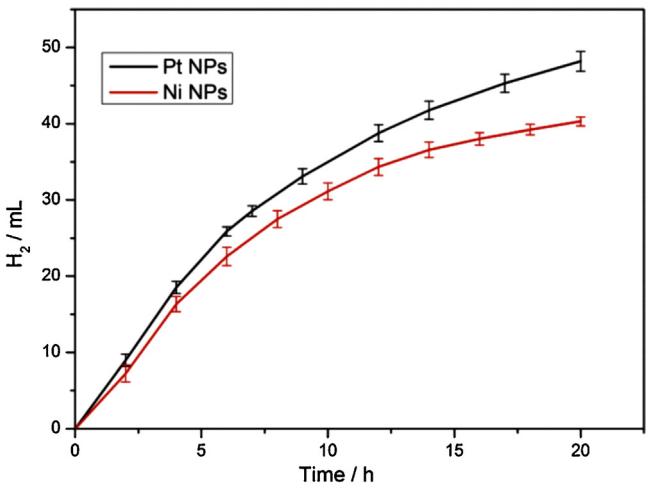

Fig. 5. Comparison of hydrogen evolution between Ni NPs (6 nm, 5.50×10^{-5} M, red line) and Pt NPs (5 nm, 5.50×10^{-5} M, black line) under visible light ($\lambda \geq 420$ nm) irradiation in 10 mL H_2O solution at pH 3.0 containing CdS NRs (1.84×10^{-4} M), lactic acid (1 mL; 10%, v/v). (For interpretation of the references to color in text, the reader is referred to the web version of this article.)

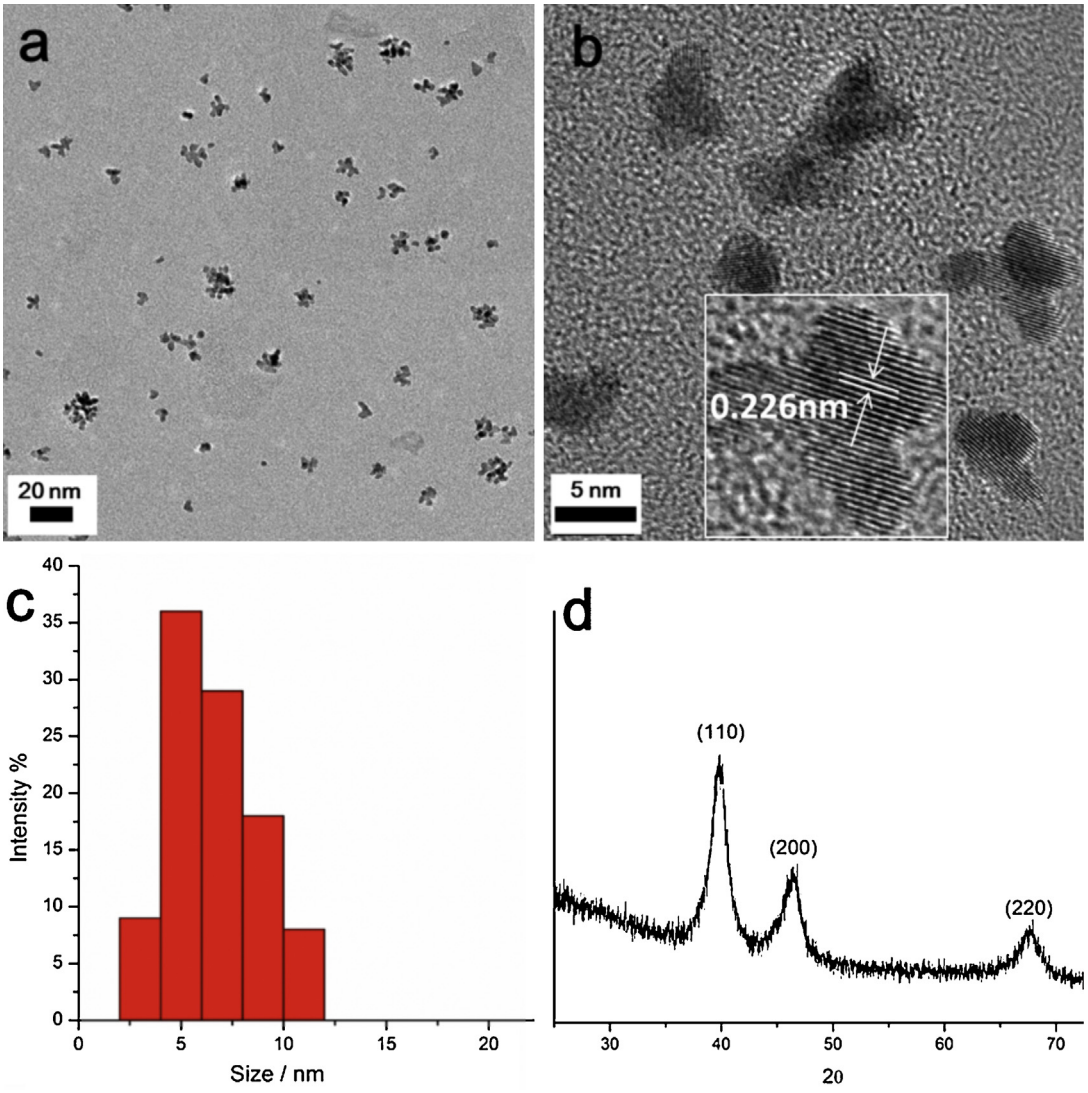

Fig. 4. (a) TEM, (b) HRTEM images of Pt NPs, (c) DLS measurements, and (d) XRD pattern of Pt NPs.

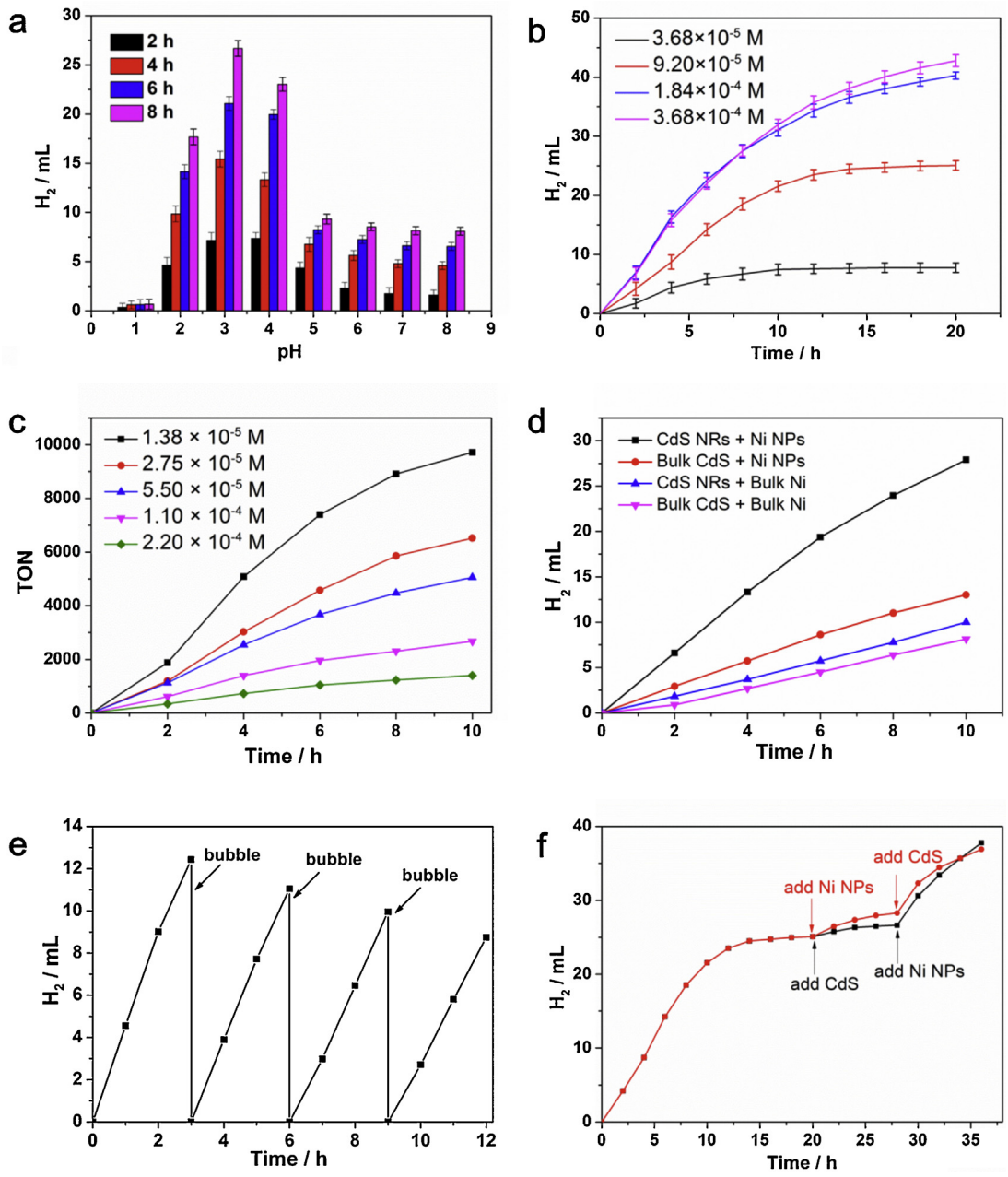

Fig. 6. (a) Photocatalytic H_2 evolution at different pH values in 10 mL H_2O: CdS NRs (1.84×10^{-4} M), Ni NPs (5.50×10^{-5} M), lactic acid (1 mL; 10%, v/v); (b) the dependence of H_2 evolution at pH 3.0 on the concentration of CdS NRs from 3.68×10^{-5} M to 3.68×10^{-4} M at fixed Ni NPs (5.50×10^{-5} M), lactic acid (10%, v/v); (c) Ni NPs from 1.38×10^{-5} M to 2.2×10^{-4} M at fixed CdS NRs (1.84×10^{-4} M), lactic acid (10%, v/v); (d) activity comparison between colloidal and bulk system, both of that containing CdS (3.68×10^{-6} mol), Ni (5.50×10^{-7} mol) and 1 mL LA (10%, v/v) at pH 3.0; (e) time course of photocatalytic H_2 production for the system containing CdS NRs (3.68×10^{-4} M), Ni NPs (5.50×10^{-5} M), lactic acid (1 mL; 10%, v/v). The reaction system was bubbled with N_2 for 30 min every 3 h to remove the H_2 inside. (f) Two parallel hydrogen production systems containing CdS NRs (9.20×10^{-5} M), Ni NPs (5.50×10^{-5} M), lactic acid (1 mL; 10%, v/v) at pH 3.0 in 10 mL H_2O. CdS NRs and Ni NPs were added at the indicated times, respectively.

Fig. 6b clearly shows the dependence of hydrogen evolution over time on the concentration of CdS NRs. Increasing the concentration of CdS NRs from 3.68×10^{-5} M to 1.84×10^{-4} M enhanced remarkably both the rate of H_2 evolution and the total amount of H_2 evolved from the system at pH value 3.0, containing 5.50×10^{-5} M Ni NPs and 1 mL (10%, v/v) LA. Higher concentration of CdS NRs as photosensitizers would absorb more photons to generate multiple excited electrons and thus lead to higher amount of H_2 evolution. However, when further increasing the concentration of CdS NRs from 1.84×10^{-4} M to 3.68×10^{-4} M, hydrogen production efficiency remained almost the same at the first 10 h. Hydrogen evolution rates do not scale linearly with further increase in CdS NRs concentration, which may be attributed to the limited concentration of Ni NPs catalysts. On the other hand, the amount of Ni NPs also clearly affects the amount and rate of photocatalytic H_2 production when the concentrations of both CdS NRs and LA were fixed. The initial rate of H_2 generation has a first-order dependence on Ni NPs concentration (Fig. S4). At 1.38×10^{-5} M Ni NPs, this system achieved the maximum TON 9710 mol H_2 per mole of catalyst after 10 h of irradiation and the TOF was 1232 mol of H_2 per mole catalyst per hour at the first 6 h (Fig. 6c), which displayed high amount and rate of hydrogen evolution compared

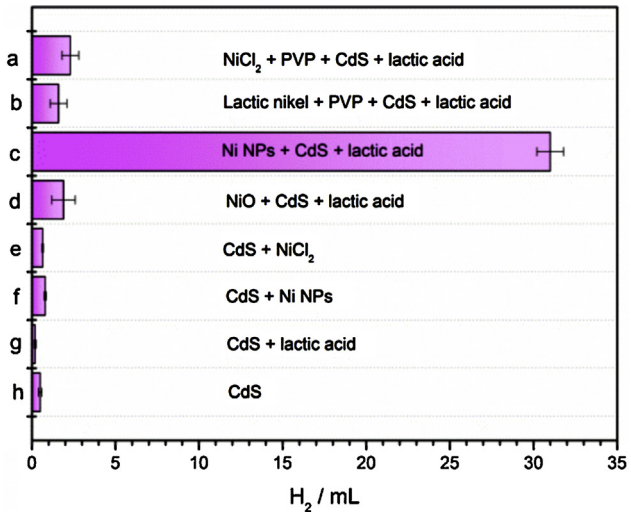

Fig. 7. Active comparison of the systems with different components. All the experiments were performed in 10 mL aqueous solution at pH 3.0 for 10 h visible light ($\lambda \geq 420$ nm) irradiation. The concentrations of the different components are as follows: CdS NRs (1.84×10^{-4} M), Ni NPs (5.50×10^{-5} M), Ni^{2+} (5.50×10^{-5} M), NiO (4.05×10^{-5} mol), lactic acid (10%, v/v), PVP (3 mg). (a) $NiCl_2{\cdot}6H_2O$, PVP, CdS NRs and lactic acid; (b) lactic nickel, PVP, CdS NRs and lactic acid; (c) Ni NPs, CdS NRs and lactic acid; (d) NiO, CdS NRs and lactic acid; (e) $NiCl_2{\cdot}6H_2O$, CdS NRs; (f) Ni NPs and CdS NRs; (g) CdS NRs and lactic acid; (h) CdS NRs.

to that reported in the literature [31,42]. To show the important role of colloidal Ni NPs and CdS NRs in the photocatalytic reactions, comparison experiments with bulk CdS or bulk Ni (0) have been performed. The synthetic methods and characterizations of bulk CdS and bulk Ni are displayed in Fig. S5. As shown in Fig. 6d, the system containing CdS NRs–Ni NPs shows the highest H_2-production rate among the four samples, whereas bulk CdS–Ni NPs and CdS NRs-bulk Ni (0) have the middle values, respectively. Bulk CdS-bulk Ni (0) system shows the lowest value. So it is clear that "soluble" colloidal Ni nanoparticles and CdS NRs demonstrate unique catalytic activity in this "homogeneous" system compared with the traditional heterogeneous CdS and Ni (0).

Recycling rest was performed to evaluate the stability of the photocatalytic system. Fig. 6e displays the H_2-production performance for the system containing 3.68×10^{-4} M CdS NRs, 5.50×10^{-5} M Ni NPs and 1 mL LA (10%, v/v). After four recycles, the H_2 evolution rate can reach up to 70% of the initial rate and more than 42 mL H_2 produced, the decrease in rate of H_2-production was attributed to photocorrosion of CdS NRs and Ni the slow transformation of Ni NPs into Ni^{2+} under the acidic conditions. However, the significance of the dramatic increase of photocatalytic hydrogen evolution efficiency in the presence of such low concentration of Ni NPs is intriguing, and higher hydrogen production activity is broad prospect as further tune the stability of quantum dots

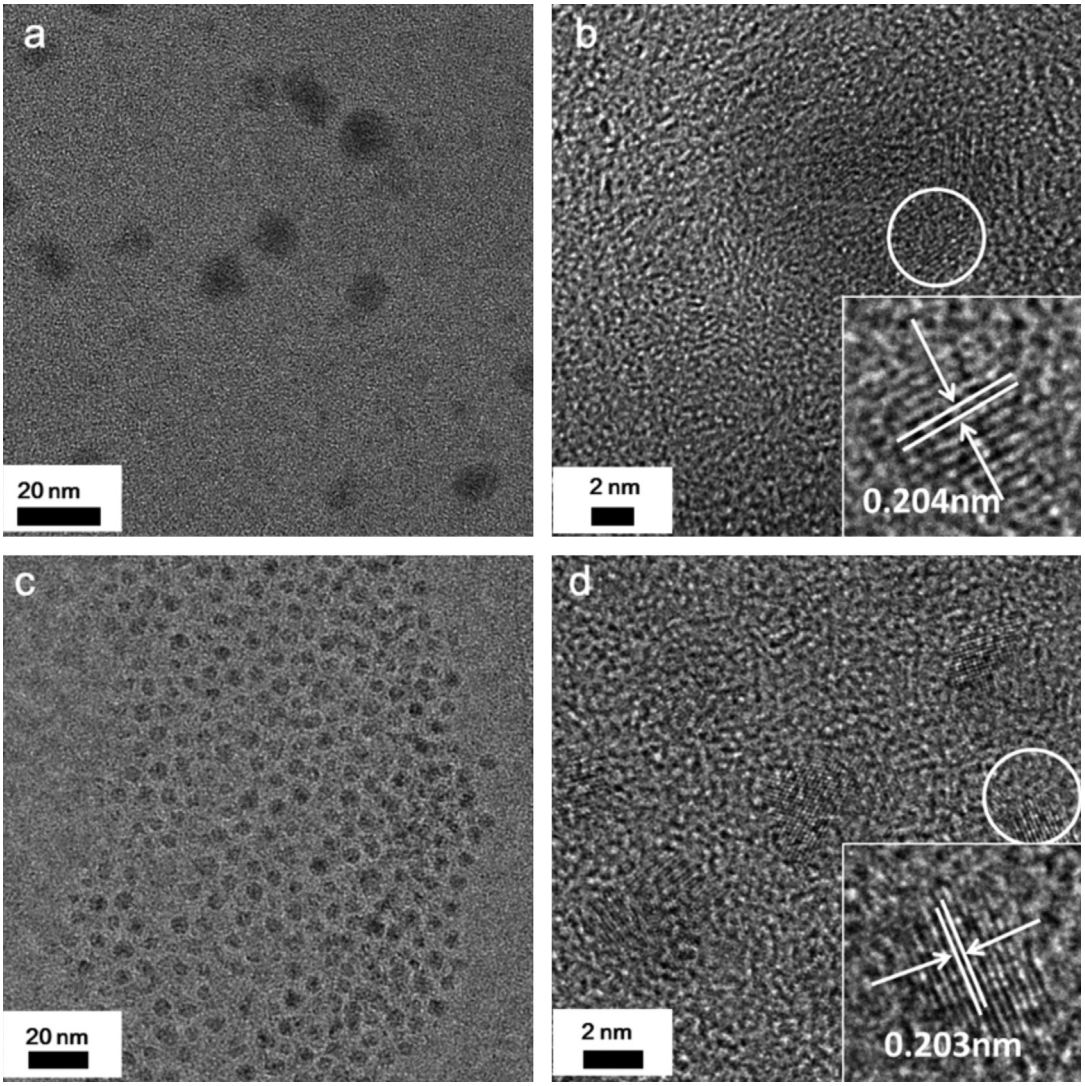

Fig. 8. TEM and HRTEM images of (a and b) Fe NPs and (c and d) Co NPs.

photosensitizer and the composition structure of non-precious metals.

As shown in Fig. 6f, over 25 mL H_2 was produced at CdS NRs concentration of 9.20×10^{-5} M and Ni NPs of 5.50×10^{-5} M after 15 h of irradiation, by which time photocatalytic hydrogen evolution also reached to a plateau. In order to quantify the role of photosensitizer and catalyst in the system, additional aliquots of CdS NRs and Ni NPs were separately added into the parallel systems at 20 h; partially restored photocatalytic activities could be observed in both instances but with the system incorporating additional Ni NPs exhibiting a higher resumed activity. Furthermore, as shown in Fig. 6f, a further reverse adding of Ni NPs and CdS NRs at 28 h could dramatically restore most of the parallel systems' activity and the system introducing Ni NPs catches up and excels in hydrogen evolution efficiency over the other system. Therefore, these experimental results indicates that although both CdS NRs and Ni NPs are responsible for the decrease in efficiency which is common in most photocatalytic systems, slow Ni NPs transformation into Ni^{2+} in the acidic aqueous solution is more culpable for the loss of activity. However, H_2 produced by the chemical redox reaction of Ni NPs with H^+ is negligible due to the little amount of Ni NPs (5.50×10^{-7} mol), which further confirms that the highly efficient activity with the high amount and fast rate of hydrogen evolution in our system is mediated by Ni NPs as catalyst in photocatalytic process.

As reported in the literature [19], Ni^{2+} could form a hybrid catalyst on the surface of CdSe/CdS core/shell QDs. In order to clarify the role of Ni^{2+} in our system, control experiments with $NiCl_2{\cdot}6H_2O$ and lactic nickel (5.50×10^{-5} M Ni^{2+}) were added in place of Ni NPs into the photocatalytic system, which displayed much lower H_2 production efficiency than system with Ni NPs as catalyst under otherwise same experimental conditions (Fig. 7). As Ni NPs are known to be easily oxidized under ambient environmental conditions, we also prepared NiO nanoparticles according to the literature methods (Figs. S6 and S7) [54] and used as catalyst to replace Ni NPs in the present system. As illustrated in Fig. 7d, hydrogen evolution with NiO exhibited much poorer efficiency than Ni NPs even if in higher molar amount. These results prove that Ni NPs was an efficient catalyst and preclude the effect of oxidized Ni NPs on the photocatalytic hydrogen evolution in our system.

Furthermore, other earth abundant metal nanoparticles like Fe and Co nanoparticles were also tested as catalysts in place of Ni NPs for photocatalytic hydrogen evolution in the present system. Highly monodispersed nanoparticles of Co and Fe nanoparticles with ca. 5 nm and 12 nm in diameter were prepared and characterized by TEM and HRTEM images, respectively (Fig. 8). In the HRTEM images (Fig. 8b), we observe a regular 0.204 nm basal spacing which is consistent with the spacing of a crystal lattice plane (1 1 0) of α-Fe. Fig. 8d shows the HRTEM image of Co NPs, the d spacing of 0.203 nm can be assigned to the characteristic pattern of fcc cobalt metal. DLS tests (Fig. S8) showed that the size of the as-prepared nanoparticles corresponded well with the measurements of TEM. The photocatalytic hydrogen evolution results demonstrated that Fe and Co nanoparticles can also be used as catalysts for hydrogen production under the same experimental conditions as Ni NPs. However, the catalytic activities of both Fe and Co nanoparticles were rather modest compared with Ni NPs as indicated in Fig. 9.

Under visible light irradiation, CdS NRs absorbed visible light and generated excited electrons and holes [43], the photo-excited electrons in the conduction band of CdS can easily transfer to the surface of Ni NPs in the aqueous solution. And lactic acid in the photocatalytic system served as the sacrificial electron donor and scavenged the generated holes [39]. As indicated in the literature studies, the fluorescence intensity clearly corresponds with

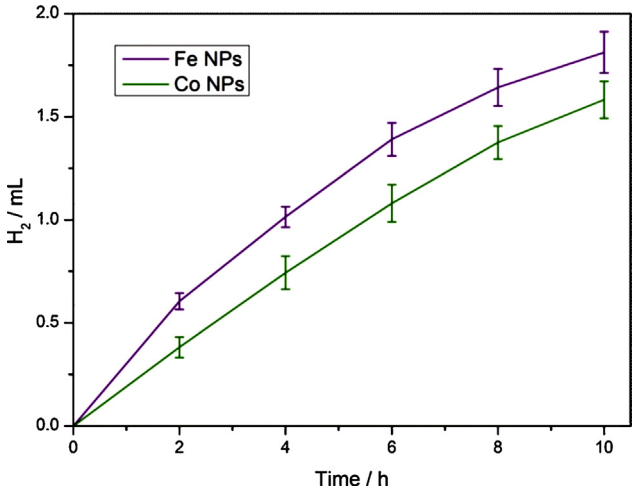

Fig. 9. Time courses of hydrogen evolution under visible light irradiation in 10 mL H_2O solution at pH 3.0 containing CdS NRs (1.84×10^{-4} M), lactic acid (1 mL; 10%, v/v) and Fe NPs (5.50×10^{-5} M) or Co NPs (5.50×10^{-5} M) at 298 K.

the product of the excited electrons and holes populations [48]. A series of fluorescence quenching studies were carried out to reflect the electron transfer processes from CdS NRs to metal nanoparticles. The fluorescence of CdS NRs (excited at 365 nm) can be effectively quenched by 6 nm Ni NPs following a linear Stern–Volmer plot with a quenching rate constant of $k_q = 36.349$. Fluorescence quenching by Pt, Fe, Co used as catalyst in our photocatalytic system, were also studied and experimental results indicated that their quenching rate constant were at the same order as that of 6 nm Ni NPs, with 5 nm Pt NPs having a $k_q = 64.892$ (Figs. 10, S9 and Table S1). The fluorescence quenching by LA was also performed and a quenching rate constant of $k_q = 5.632$ was obtained, which is one order lower than that of the metal catalysts (Fig. S10).

Photoelectrochemical measurement was also used to study the excitation and transfer of charge carriers photogenerated in the CdS NRs-Ni NPs system. Fig. 11 shows the transient photocurrent responses of the CdS NPs, CdS NRs–Ni NPs and CdS NRs–Pt NRs as the irradiation time. The CdS NRs–Pt NPs electrode showed highest photocurrent intensity, and the photocurrent densities of CdS NPs–Ni NPs are higher than that of CdS NRs, indicating the better charge separation and transfer from the colloid CdS NPs to Ni NPs catalysts. The photoelectrochemical experiments demonstrate that non-precious metal Ni can also effective transfer and separate the charge photoexcited in the CdS semiconductor to suppress the recombination of charge carriers, and the transient photocurrent response results also displayed the good photoexcited current stability as the irradiation time, which are well consistent with the photocatalytic-activity measurements and our above discussions.

Based on these results, a concise possible mechanism tentatively proposed for the photocatalytic process concerning photoexcited electron transfer from CdS NRs to Ni NPs for light-driven hydrogen production is presented in Fig. 12. Adding Ni NPs into the photocatalytic system containing CdS NRs was found to exhibit dramatically enhanced hydrogen evolution, which can be attributed to the efficient photoexcited electron flow from the conduction band of QDs to the surface of active metal catalyst, which is efficient for capturing electrons and preventing photogenerated electron-hole recombination and meanwhile a highly effective catalyst for mediating hydrogen production reaction under the photocatalytic conditions. The photogenerated holes can be consumed by sacrificial electron donor (LA) which also prevents the CdS NRs from photo-corrosion.

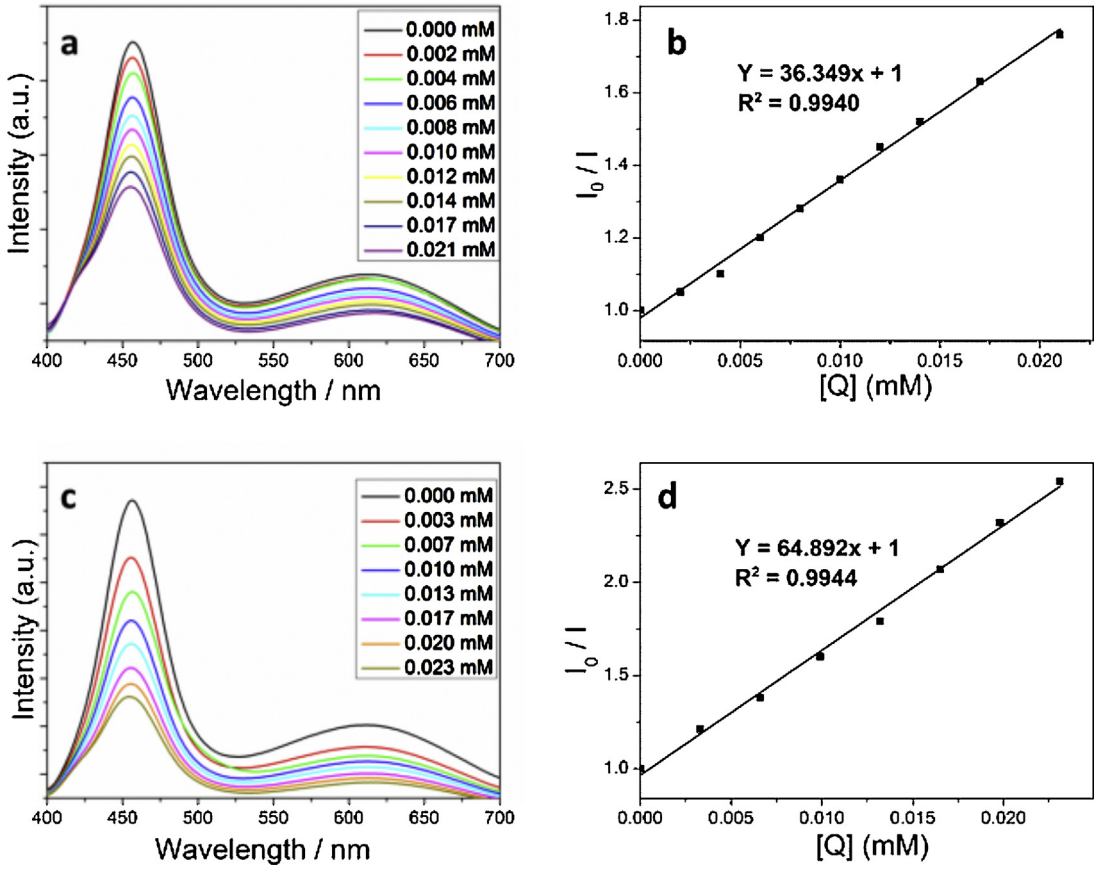

Fig. 10. Stern–Volmer plot (b and d) of the emission quenching (a and c) of CdS NRs solution (1.38×10^{-5} M) by (a and b) Ni NPs and (c and d) Pt NPs, respectively, in 3 mL H_2O at pH 3.0. The best-fit equation of Stern–Volmer plot is indicated in the picture.

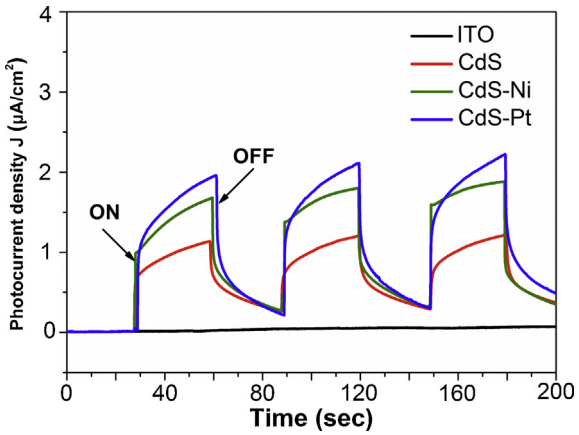

Fig. 11. Transient photocurrent responses of CdS NRs (red line), CdS NRs-Ni NPs (green line) and CdS NRs-Pt NPs (blue line) in a 0.5 M Na_2SO_4 aqueous solution under visible-light irradiation at 0.0 V using Ag/AgCl as a reference electrode. (For interpretation of the references to color in text, the reader is referred to the web version of this article.)

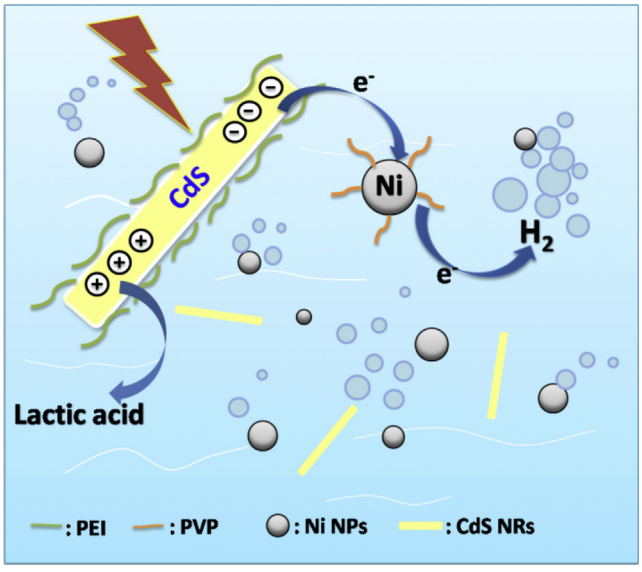

Fig. 12. A possible mechanism for the photocatalytic hydrogen evolution.

4. Conclusions

A highly efficient noble-metal-free photocatalytic system in aqueous solution was explored for hydrogen evolution using nanocrystal CdS nanorods photosensitizer coupled with size-controlled water-soluble colloidal Ni NPs catalyst and LA sacrificial electron donor. The system displayed highly efficient visible light ($\lambda \geq 420$ nm) induced activity for hydrogen evolution. The highest efficiency was obtained with Ni NPs of 6 nm size, which could reach up to 80% of that catalyzed by the well-known Pt nanoparticles (5 nm) using the same catalyst molar amount, which is of great value based on economic concerns that Pt is noble and far more expensive than Ni. The system demonstrated that Ni NPs had high H_2 evolution efficiency with 9710 TON (relative to Ni NPs) after 10 h of illumination and a TOF of 1232 mol H_2 per mole Ni NPs per hour in the first 6 h. Control experiments showed that the visible light-driven H_2 production efficiency was very dependent on the solution pH value, the concentrations both of the CdS NRs and Ni NPs as well. Although the Ni NPs undergo slow transformation into Ni^{2+} under the acidic conditions, the significance of the dramatic increase of photocatalytic hydrogen evolution efficiency in the presence of such low concentrations of Ni NPs is intriguing, and higher hydrogen production activity is broad prospect as further tune the stability of quantum dots photosensitizer and the composition structure of non-precious metals. This work demonstrates a viable strategy to achieve highly efficient hydrogen production with earth abundant inorganic catalysts in aqueous solution and provides some novel notions of efficiently harnessing solar energy for photocatalytic applications.

Acknowledgements

This work was financially supported by the National Key Basic Research Program of China (973 Program 2013CB834804, 2013CB632403) and the Ministry of Science and Technology (2012DFH40090). We thank the Natural Science Foundation of China (21107117, 21273257, 21353002, 21371175), Beijing Natural Science Foundation (2132057) for financial support. Y. C. acknowledges Chinese Academy of Science (100 Talents Program) for funding support.

Appendix A. Supplementary data

Supplementary data associated with this article can be found, in the online version, at http://dx.doi.org/10.1016/j.apcatb.2014.07.014.

References

[1] A.J. Esswein, D.G. Nocera, Chem. Rev. 107 (2007) 4022–4047.
[2] R.M. Navarro, M.C. Sánchez-Sánchez, M.C. Alvarez-Galvan, F.D. Valle, J.L.G. Fierro, Energy Environ. Sci. 2 (2009) 35–54.
[3] A.J. Bard, M.A. Fox, Acc. Chem. Res. 28 (1995) 141–145.
[4] K. Maeda, K. Teramura, D. Lu, T. Takata, N. Saito, Y. Inoue, K. Domen, Nature 440 (2006), 295-295.
[5] W.T. Eckenhoff, R. Eisenberg, Dalton. Trans. 41 (2012) 13004–13021.
[6] P.D. Tran, L.H. Wong, J. Barber, J.S.C. Loo, Energy Environ. Sci. 5 (2012) 5902–5918.
[7] X. Chen, S.S. Mao, Chem. Rev. 107 (2007) 2891–2959.
[8] A. Kubacka, M. Fernández-García, G. Colón, Chem. Rev. 112 (2012) 1555–1614.
[9] H. Tong, S. Ouyang, Y. Bi, N. Umezawa, M. Oshikiri, J. Ye, Adv. Mater. 24 (2012) 229–251.
[10] H.G. Yang, C.H. Sun, S.Z. Qiao, J. Zou, G. Liu, S.C. Smith, H.M. Cheng, G.Q. Lu, Nature 453 (2008) 638–641.
[11] X.J. Lv, S.X. Zhou, C. Zhang, H.X. Chang, Y. Chen, W.F. Fu, J. Mater. Chem. 22 (2012) 18542–18549.
[12] X.J. Lv, W.F. Fu, H.X. Chang, H. Zhang, J.S. Cheng, G.J. Zhang, Y. Song, C.Y. Hu, J.H. Li, J. Mater. Chem. 22 (2012) 1539–1546.
[13] K. Maeda, T. Takata, M. Hara, N. Saito, Y. Inoue, H. Kobayashi, K. Domen, J. Am. Chem. Soc. 127 (2005) 8286–8287.
[14] J.H. Bang, R.J. Helmich, K.S. Suslick, Adv. Mater. 20 (2008) 2599–2603.
[15] J.S. Hu, L.L. Ren, Y.G. Guo, H.P. Liang, A.M. Cao, L.J. Wan, C.L. Bai, Angew. Chem. Int. Ed. 44 (2005) 1269–1273.
[16] R.C. Pawar, C.S. Lee, Appl. Catal. B: Environ. 144 (2014) 57–65.
[17] B. Wang, D. Guan, Z. Gao, J. Wang, Z. Li, W. Yang, L. Liu, Mater. Chem. Phys. 141 (2013) 1–8.
[18] Z. Han, F. Qiu, R. Eisenberg, P.L. Holland, T.D. Krauss, Science 338 (2012) 1321–1324.
[19] Z.J. Li, J.J. Wang, X.B. Li, X.B. Fan, Q.Y. Meng, K. Feng, B. Chen, C.H. Tung, L.Z. Wu, Adv. Mater. 25 (2013) 6613–6618.
[20] J. Zhang, Y. Wang, J. Jin, J. Zhang, Z. Lin, F. Huang, J. Yu, ACS Appl. Mater. Interfaces 5 (2013) 10317–10324.
[21] Z.J. Li, X.B. Li, J.J. Wang, S. Yu, C.B. Li, C.H. Tung, L.Z. Wu, Energy Environ. Sci. 6 (2013) 465–469.
[22] C.B. Li, Z.J. Li, S. Yu, G.X. Wang, F. Wang, Q.Y. Meng, B. Chen, K. Feng, C.H. Tung, L.Z. Wu, Energy Environ. Sci. 6 (2013) 2597–2602.
[23] J.X. Jian, Q. Liu, Z.J. Li, F. Wang, X.B. Li, C.B. Li, B. Liu, Q.Y. Meng, B. Chen, K. Feng, C.H. Tung, L.Z. Wu, Nat. Commun. 4 (2013) 498–502.
[24] J. Huang, K.L. Mulfort, P. Du, L.X. Chen, J. Am. Chem. Soc. 134 (2012) 16472–16475.
[25] B. O'Regan, M. Gratzel, Nature 353 (1991) 737–740.
[26] H. Zhu, N. Song, H. Lv, C.L. Hill, T. Lian, J. Am. Chem. Soc. 134 (2012) 11701–11708.
[27] A.J. Nozik, M.C. Beard, J.M. Luther, M. Law, R.J. Ellingson, J.C. Johnson, Chem. Rev. 110 (2010) 6873–6890.
[28] A. Hagfeldt, G. Boschloo, L. Sun, L. Kloo, H. Pettersson, Chem. Rev. 110 (2010) 6595–6663.
[29] D.V. Talapin, J.S. Lee, M.V. Kovalenko, E.V. Shevchenko, Chem. Rev. 110 (2009) 389–458.
[30] X. Li, M. Wang, D. Zheng, K. Han, J. Dong, L. Sun, Energy Environ. Sci. 5 (2012) 8220–8224.
[31] P. Du, R. Eisenberg, Energy Environ. Sci. 5 (2012) 6012–6021.
[32] W.R. McNamara, Z. Han, P.J. Alperin, W.W. Brennessel, P.L. Holland, R. Eisenberg, J. Am. Chem. Soc. 133 (2011) 15368–15371.
[33] H.Y. Wang, G. Si, W.N. Cao, W.G. Wang, Z.J. Li, F. Wang, C.H. Tung, L.Z. Wu, Chem. Commun. 47 (2011) 8406–8408.
[34] Z. Han, W.R. McNamara, M.S. Eum, P.L. Holland, R. Eisenberg, Angew. Chem. Int. Ed. 51 (2012) 1667–1670.
[35] F. Wang, W.G. Wang, H.Y. Wang, G. Si, C.H. Tung, L.Z. Wu, ACS Catal. 2 (2012) 407–416.
[36] S. Fukuzumi, D. Hong, Y. Yamada, J. Phys. Chem. Lett. 4 (2013) 3458–3467.
[37] H. Kotani, R. Hanazaki, K. Ohkubo, Y. Yamada, S. Fukuzumi, Chem. Eur. J. 17 (2011) 2777–2785.
[38] J. Ran, J. Yu, M. Jaroniec, Green Chem. 13 (2011) 2708–2713.
[39] W. Zhang, Y. Wang, Z. Wang, Z. Zhong, R. Xu, Chem. Commun. 46 (2010) 7631–7633.
[40] J. Hong, Y. Wang, Y. Wang, W. Zhang, R. Xu, ChemSusChem 6 (2013) 2263–2268.
[41] C. Wang, S. Cao, W.F. Fu, Chem. Commun. 49 (2013) 11251–11253.
[42] Y. Yamada, T. Miyahigashi, H. Kotani, K. Ohkubo, S. Fukuzumi, Energy Environ. Sci. 5 (2012) 6111–6118.
[43] T. Jia, A. Kolpin, C. Ma, R.C.T. Chan, W.M. Kwok, S.C.E. Tsang, Chem. Commun. 50 (2014) 1185–1188.
[44] Y. Shemesh, J.E. Macdonald, G. Menagen, U. Banin, Angew. Chem. Int. Ed. 50 (2011) 1185–1189.
[45] H.N. Kim, T.W. Kim, I.Y. Kim, S.J. Hwang, Adv. Funct. Mater. 21 (2011) 3111–3118.
[46] X. Chen, S. Shen, L. Guo, S.S. Mao, Chem. Rev. 110 (2010) 6503–6570.
[47] X. Zong, H. Yan, G. Wu, G. Ma, F. Wen, L. Wang, C. Li, J. Am. Chem. Soc. 130 (2008) 7176–7177.
[48] H.W. Tseng, M.B. Wilker, N.H. Damrauer, G. Dukovic, J. Am. Chem. Soc. 135 (2013) 3383–3386.
[49] Z. Zhuang, X. Lu, Q. Peng, Y. Li, J. Am. Chem. Soc. 132 (2010) 1819–1821.
[50] Y. Chen, D.L. Peng, D. Lin, X. Luo, Nanotechnology 18 (2007) 505703–505708.
[51] S. Peng, C. Wang, J. Xie, S. Sun, J. Am. Chem. Soc. 128 (2006) 10676–10677.
[52] Y. Bao, W. An, C.H. Turner, K.M. Krishnan, Langmuir 26 (2010) 478–483.
[53] Z. Fang, Y. Wang, J. Song, Y. Sun, J. Zhou, R. Xu, H. Duan, Nanoscale 5 (2013) 9830–9838.
[54] D. Tao, F. Wei, Mater. Lett. 58 (2004) 3226–3228.
[55] X. Zong, Y. Na, F. Wen, G. Ma, J. Yang, D. Wang, Y. Ma, M. Wang, L. Sun, C. Li, Chem. Commun. (2009) 4536–4538.
[56] S. Zhou, B. Varughese, B. Eichhorn, G. Jackson, K. McIlwrath, Angew. Chem. Int. Ed. 44 (2005) 4539–4543.
[57] K.A. Brown, S. Dayal, X. Ai, G. Rumbles, P.W. King, J. Am. Chem. Soc. 132 (2010) 9672–9680.
[58] F. Wang, W.G. Wang, X.J. Wang, H.Y. Wang, C.H. Tung, L.Z. Wu, Angew. Chem. Int. Ed. 50 (2011) 3193–3197.